Available online at www.sciencedirect.com
SCIENCE DIRECT
ELSEVIER
Journal of the European Ceramic Society 26 (2006) 967–980
ECERS
www.elsevier.com/locate/jeurceramsoc

Time-of-flight secondary ion mass spectrometry as a tool for studying segregation phenomena at nickel–YSZ interfaces

K. Norrman [a,*], K. Vels Hansen [b], M. Mogensen [b]

[a] *Danish Polymer Centre, Risø National Laboratory, DK-4000 Roskilde, Denmark*
[b] *Materials Research Department, Risø National Laboratory, DK-4000 Roskilde, Denmark*

Received 1 August 2004; received in revised form 24 November 2004; accepted 5 December 2004
Available online 5 March 2005

Abstract

Through a study of Ni–YSZ interfaces it is shown that time-of-flight-secondary ion mass spectrometry (TOF-SIMS) is a powerful and convenient tool for the analysis of ultra thin layers of segregated material at the interfaces and on free surfaces. Two different types of Ni, "pure Ni" (99.995% Ni) and "impure Ni" (99.8% Ni) were investigated. The contact areas on the YSZ and areas outside the contacts were examined with XPS and TOF-SIMS. The impure nickel causes a relatively larger amount of impurities to accumulate at the contact area, e.g. oxides of Mn, Ti, Si and Na. Some impurities migrate to the area outside the contact area. Even though on a larger scale the impurities seem to be homogeneously distributed, detailed analyses in and outside the contact area show the presence of impurity particles, and that the surface species are inhomogeneously distributed amongst the different grains. The extremely low detection limit, the small probe depth, the image capability, and the ease of elemental identification make TOF-SIMS an obvious choice as an analytical tool for studying segregation phenomena at metal–ceramic interfaces such as Ni–YSZ interfaces. XPS, being a quantitative technique, was used as a complementary technique to TOF-SIMS, which is not directly a quantitative technique.

Keywords: Interface; Segregation; Fuel cells; ZrO_2; YSZ–Ni; SIMS

1. Introduction

The purpose of this paper is to show that time-of-flight-secondary ion mass spectrometry (TOF-SIMS) is a suitable tool for analysing ultra thin segregated layers of impurities on surfaces and interfaces. As an example, we have chosen the Ni-yttria stabilised zirconia (YSZ) system, which is very important within the area of solid oxide fuel cells (SOFC). Most developers of SOFC use YSZ as the electrolyte and a mixture of nickel and YSZ as the fuel electrode, i.e. the anode.[1] Even though this electrode has proven to be applicable for SOFC systems with long durability[2] it has been argued that the polarisation resistance, R_p, ought to be much smaller than what is actually measured.[3,4] It is important to decrease the internal resistance of the SOFC in order to decrease the cost of the SOFC system. The electrochemical oxidation of H_2 to H_2O is supposed to be fastest if the H_2 molecules dissociate into protons, H^+, on the surface of the Ni particles[4–6] and then diffuse across the three phase boundary (TPB) line, where gas, electron-conducting Ni and ion-conducting YSZ meet each other. The H^+ ions then diffuse further onto the surface of the YSZ electrolyte, where they form water molecules by reaction with the oxide ions. Another possible reaction path is diffusion of protons through the bulk of the Ni particles, across the Ni–YSZ interface, and further through the bulk YSZ by hopping from one oxide ion to another[7,8] until the protons reach the YSZ surface, where the proton containing OH^- ions combine and escape in the form of water.[4]

The fact that the R_p of the Ni–YSZ is orders of magnitude too high[4] together with the observation that different kinetics

* Corresponding author. Tel.: +45 46 77 47 93; fax: +45 46 77 47 91.
E-mail addresses: kion.norrman@risoe.dk (K. Norrman), karin.vels@risoe.dk (K.V. Hansen), mogens.mogensen@risoe.dk (M. Mogensen).

0955-2219/$ – see front matter © 2005 Elsevier Ltd. All rights reserved.
doi:10.1016/j.jeurceramsoc.2004.12.030

are reported by every research group, led us to the hypothesis that some kind of barrier for the transport of protons from the Ni to the YSZ existed, and this barrier was very dependent on the exact type of raw materials and fabrication procedure.[9] This hypothesis was confirmed experimentally both for Ni–YSZ cermets[10] and for so-called point electrodes[11,12] with only one contact interface between Ni and YSZ. The barrier was of the same type of Si containing glassy phases as observed previously on YSZ grain boundaries[13] and free surfaces.[14] It had also previously been indicated that such segregated phases was impeding the oxygen reduction reaction in case of platinum on YSZ.[15] Even though the YSZ powder contains only a very low concentration of impurities, it is well documented in the literature that both impurity and Y-segregation to the surface and sub-surface region occur, see e.g. Refs.[13,14] The NiO powder used for Ni–YSZ cermet anodes also contains some impurities, which contribute. Impurities were seen to migrate to the Ni–YSZ interface and external Ni and YSZ surfaces for Ni-point electrodes both with electrodes consisting of 99.8% Ni (impure Ni) and with the much purer electrodes consisting of 99.995% Ni (pure Ni). The impurities were also accumulating in a ridge on the TPB. A clear difference in the electrochemical performance between samples with 99.8% nickel electrodes and 99.995% nickel electrodes was found, and during anodic polarisation the best pure electrodes were at least a factor of 10 better than the best impure electrodes.[16]

The interfaces between the Ni and YSZ are, due to the point electrode geometry, very small areas in the order of 0.001–0.002 cm^2, and since the materials are relatively pure, we need to detect very small amounts of impurities. This combination poses a problem for many analysis techniques. Further, the size of the reaction zone width along the TPB seems to be less than 1 μm, and the exact size is unknown.[3] Thus, there is a strong need for analytical tools which may be used to study the composition on surfaces and interfaces with a resolution on the nanometer (nm) scale in the lateral direction and with one atomic layer resolution on the surface/interface, because even a partial coverage of an interface with impurities may impede significantly the ionic transport across the interface.

Based on the above we decided to explore the possibilities of TOF-SIMS by analysing two Ni–YSZ contact areas on samples that were heat-treated at 1000 °C. The samples were nominally equal to the previous samples[16] on which we performed electrochemical measurements.

This paper shows that the TOF-SIMS is a convenient and powerful tool for investigation of the phenomena associated with the SOFC electrode barriers, which originate from segregation of cell components (such as yttria) and impurities to the electrolyte/electrode interface. TOF-SIMS is in particular helpful when it is used in combination with other tools like scanning electron microscopy (SEM), X-ray photoelectron spectroscopy (XPS), and atomic force microscopy (AFM). This paper is the first in (hopefully) a series of papers in which we study the Ni–YSZ system with TOF-SIMS analyses as a supplement to other previously used analysis techniques.

Before describing the TOF-SIMS technique a brief summary of the literature, in which other techniques than TOF-SIMS have been used to study the composition of YSZ interfaces, is given.

2. Analytical techniques previously used for studies of YSZ interfaces

Investigations of the YSZ interfaces have been done by means of transmission electron microscopy (TEM) combined with energy dispersive spectrometry (EDS) or electron energy loss spectroscopy,[17–19] and this seems to be the only appropriate method for fine structured Ni–YSZ cermets and other composite electrodes. The problem with TEM of Ni–YSZ cermets is that it is very difficult to correlate the performance of the macroscopic electrode (consisting of thousands of Ni–YSZ particle contacts) with the very localised TEM analysis results, and the preparation of the sample for TEM analysis is extremely resource consuming. The spatial resolution for TEM imaging is 0.1–0.2 nm for optimal conditions. The spatial resolution for chemical analysis (PEELS) is from 0.5 nm and up, depending on the sample thickness and elements to be analysed.

Other techniques, which have been used to characterize interfaces of ZrO_2-based ceramics, are XPS and Auger electron spectroscopy (AES and XAES).[13,20] For the study of interfacial chemistry, quantitative elemental analysis is important. XPS[21] has proven to be a useful tool for studying segregation phenomena in ceramics, and seems to be the preferred technique compared to the similar XAES technique. Besides providing element identification and quantitative information, chemical state information can be obtained. The probe depth of XPS is material and instrument dependent, but is typically 5–10 nm. XPS is more surface sensitive compared to the other above-mentioned X-ray techniques providing chemical information, with a lateral resolution of a couple of microns. The XPS can detect concentrations down to fractions of an atomic percent. XPS is often used as a complementary technique to TOF-SIMS,[22] which has a lateral resolution of about 50 nm, and a much lower detection limit, in the order of ppb.

de Ridder et al.[23,24] have presented low energy ion scattering (LEIS) studies of segregation of impurities to the surface of YSZ, which was heat-treated in air (comparable to the cathode side of the fuel cell). It was shown that even at relatively low temperatures a significant amount of impurities (Si, Ca, Na) were present at the surface, and that the segregated impurities seriously restrict oxygen exchange with the surface. The study concentrates on the YSZ alone and does not include the cathode/electrolyte interface. The LEIS analyses only the outermost atomic layer and is a quantitative technique. According to Brongersma at al.[25] the lateral resolution (the spot size) is in the order of 1 mm^2.

3. General description of the TOF-SIMS technique

TOF-SIMS is an analysis method, which analyses the outermost atomic/molecular layer of a surface. A beam of primary ions of high kinetic energy bombards the sample. This results in atoms, molecules and molecular fragments desorbing from the surface. A small fraction of these will have a negative or positive charge. These secondary ions are then accelerated up to having the same kinetic energy. Ions with the same kinetic energy but with different masses will have different velocities, and thereby different times of flight through a TOF analyser. The mass of an ion can thereby be determined from the time-of-flight. Hence, the outcome of a TOF-SIMS analysis is a surface mass spectrum.

An important aspect of the technique is that the analysis can be performed under static conditions, by the use of a subtle ion bombardment, which leaves the sample practically undamaged. This is known as static TOF-SIMS. If the analysis is expanded to involve more than a point on the surface, that is to involve several points over a given area, a chemical mapping of the surface can be performed by scanning the primary ion beam. This procedure, known as TOF-SIMS imaging, produces a visualization of the distribution of elements or chemical compounds at the surface.

The lateral resolution (the width of the primary ion beam) is ∼50 nm for low mass resolution mode (unit mass resolution below m/z ∼100) and under ideal conditions. The mass resolution ($M/\Delta M$, where M is the mass and ΔM is the peak width at 50% peak height) is (for low lateral resolution mode and for ideal conditions) typically 15,000. The high mass resolution enable exact mass determination, which combined with isotope pattern recognition, makes element and chemical compound identification fairly easy. The preparation time for a TOF-SIMS analysis is comparable to the preparation time for an XPS analysis. However, the acquisition time of a TOF-SIMS analysis is orders of magnitudes faster than that of an XPS analysis, typically in the seconds range compared to several minutes for XPS. With respect to sensitivity TOF-SIMS is again superior to XPS. The detection limit for TOF-SIMS is many magnitudes smaller than the detection limit for XPS.

XPS is often used as a complementary technique to TOF-SIMS due to the fact the XPS is a quantitative technique. The main drawback of TOF-SIMS is that it is not (directly) quantitative. Quantification of some TOF-SIMS data may be possible but this would require fabrication of well-defined standards in order to produce a calibration curve.

The fundamental reason for mass spectrometry not being directly quantitative is in principle the different response factors associated with different species, i.e. different species produce different signal intensities for equal concentrations. For surface mass spectrometry it makes more sense to use the related property termed the secondary ion yield, which is the number of secondary ions detected relative to the number of primary ions used. The secondary ion yield is influenced by several factors, which are more or less linked, e.g. ionisation probability, element type, chemical structure, surface topography, and to complicate things even more, the matrix may influence the secondary ion yield. Matrix effects prevent the signal intensities from the same type of compound on different substrates or different compounds on the same substrate to be compared. This is one of the major problems in using TOF-SIMS quantitatively.

4. Experimental

Two Ni–YSZ samples were heat-treated for 216 h at 1000 °C in 97% H_2/3% H_2O. After the heat treatment the Ni and the YSZ could easily be separated and each surface could be examined. The contact areas and areas away from the contact were then examined with TOF-SIMS and subsequently with XPS. Lastly, the contact areas were examined in the scanning electron microscope. Three reference samples were examined: (i) a polished YSZ sample and (ii) a pure and (iii) an impure nickel wire.

4.1. Ni–YSZ samples

Two samples were prepared: (i) a YSZ sample with the code 231i: YSZ in contact with a relatively impure nickel wire (99.8% Ni, Johnson Matthey) and (ii) a YSZ sample with the code 232p: YSZ in contact with relatively pure nickel wire (99.995% Ni, Puratronic, Johnson Matthey). The compositions of the impurities of the nickel wires (only a typical analysis for the impure Ni) and the YSZ powder are summarised in Table 1.

The YSZ pellets were produced from TZ-8Y powder (Tosoh Corporation), which was pressed and sintered for 2 h at 1600 °C in air. After sintering, the pellets were polished in

Table 1
Impurity content of the Ni wire and YSZ powder as stated by the vendors

Element/oxide	YSZ (TZ-8Y) powder wt.%	Ni wire (99.8%) wt.%	Ni wire (99.995%) ppm
Al_2O_3	< 0.005		
SiO_2	0.003		
Fe_2O_3	< 0.002		
Na_2O	0.060		
C		0.03	
Co		0.02	
Cu		0.03	< 1
Fe		0.05	< 3
Mg		0.01	< 1
Mn		0.15	
S		0.001	
Si		0.03	1
Ti		0.01	
Al			< 1
Ca			< 1
Ag			< 1
Mo			2
Pb			1

The TZ-8Y powder is from Tosoh and the nickel wires are from Johnson Matthey.

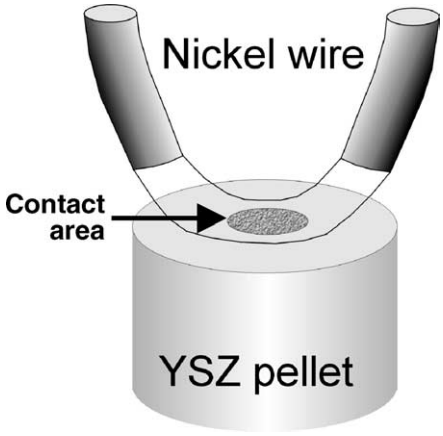

Fig. 1. Schematic of the experimental set-up of the Ni–YSZ contact showing the YSZ pellet, the nickel wire, and the contact area.

several steps ending with 1 μm diamond paste. Finally, the pellets were washed copiously with ethanol in an ultrasonic bath.

The Ni–YSZ interface was produced by pressing an electro polished bent nickel wire against the polished surface of a YSZ pellet (Fig. 1). The nickel wires were pressed against the YSZ surfaces with a load of 81 g resulting in contact areas of 0.0012 and 0.0019 cm^2, respectively.

4.2. TOF-SIMS analysis

Several areas were analysed with the TOF-SIMS: (i) a 3 mm × 3 mm scan was performed on sample 232p, (ii) 500 μm × 500 μm scans were performed in each contact area and at a distance away from the contact, (iii) 50 μm × 50 μm scans were performed in each contact area and for sample 231i at the contact area border, (iv) an area outside the contact was also analysed on sample 232p, (v) 500 μm × 500 μm and (vi) 50 μm × 50 μm scans were performed on the reference YSZ sample and (vii) 25 μm × 25 μm scans were acquired for the two reference nickel wires. To minimize contamination prior to analyses the samples were handled with clean tweezers on the side of the pellets, i.e. not on the side to be analysed.

The TOF-SIMS analyses were performed using a TOF-SIMS IV (ION-TOF GmbH, Münster, Germany) operated at a pressure of 2×10^{-8} Torr (with sample). High mass resolution spectra (low lateral resolution) were obtained using 30-ns pulses of 25-keV Ga^+ (primary ions), which were bunched to form ion packets with a nominal temporal extent of <1.1 ns at a repetition rate of 20 kHz thus yielding a target current of 1.3 pA. These primary ion conditions were used to scan a 500 μm × 500 μm area of the sample for 262 s, which corresponds to an ion dose of 8.5×10^{11} ions/cm^2. High lateral resolution images (low mass resolution) were obtained (∼200 nm) using 160-ns pulses of 25-keV Ga^+ at a repetition rate of 20 kHz thus yielding a target current of 0.6 pA. These primary ion conditions were used to scan 500 μm × 500 μm and 50 μm × 50 μm areas of the samples, which correspond to ion doses in the range 10^{11}–10^{14} ions/cm^2. An electron gun was used to minimise charging of the surface. Desorbed secondary ions were accelerated to 2 keV, mass analysed in the flight tube, and post-accelerated to 10 keV before detection.

The TOF-SIMS IV software package (version 4.0) was employed to process the data. The mass spectral data was mass calibrated in the part of the software package called IonSpec. The identity of a given signal was determined from the exact mass combined with isotope pattern recognition. The signal intensities were acquired from peak areas by integrating the mass spectral peaks. In the part of the software package called IonImage, the intensities were visualized in a 512 × 512 pixel (500 μm × 500 μm area) or a 256 × 256 pixel (50 μm × 50 μm area) image, in such that the relative pixel positions correspond to the relative positions on the analysed area on sample surface. Assigning colour shades to the intensities then results in what is known as an ion image, which displays the lateral distribution of a given species.

4.3. XPS analysis

XPS analyses were performed using an SSX-100 (Surface Science Instruments, Mountain View, CA, USA) with an Al Kα X-ray source (1486.6 eV, 15–150 W) operated at a pressure of 3×10^{-8} Torr. The analyses were performed at a 55° angle to the surface with an analyser pass energy of 150 eV. The Zr 3d line (182.2 eV) was used as a reference to correct for sample charging. This XPS is capable of analysing the very small contact areas of 150 μm × 800 μm. XPS measurements were performed in the contact area and outside it at a distance away from the contact area on both samples. The reference YSZ sample and the nickel wires were also analysed.

4.4. SEM analysis

The nickel wires corresponding to the samples 231i and 232p were examined with scanning electron microscopy (SEM, JEOL JSM-840) in order to study the surface morphologies and contact areas after the heat treatment. After the XPS and TOF-SIMS measurements the contact area on sample 231i was examined in a JEOL JSM-840 SEM. The contact area on sample 232p was examined in a JEOL JSM-5310 LVSEM. Both SEM's are equipped with EDS systems. During EDS measurements a volume of approximately 1 μm^3 is analysed.

5. Results

5.1. SEM of the nickel wires

After the heat treatment at 1000 °C for 216 h the morphologies of the nickel wires appear very different. The pure nickel wire showed only very minor changes in morphology. A few

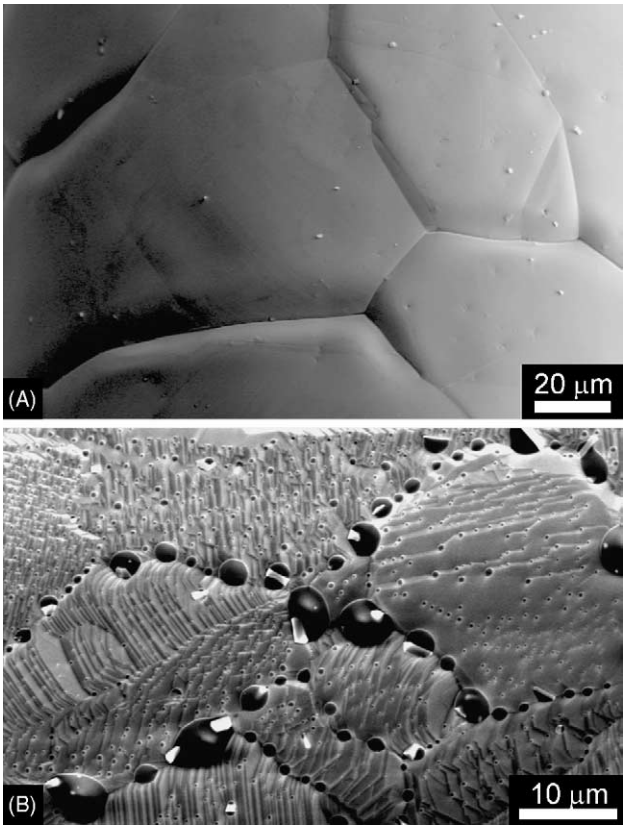

Fig. 2. Secondary electron SEM image of (A) the pure and (B) the impure nickel wire after heat treatment. Dark impurity particles are seen in the grain boundaries and also at terrace kinks in the grains of the impure nickel.

impurity particles were seen but they seemed to be alumina dust attached to the nickel during the experiment (Fig. 2A). On the impure nickel wire, large spherical particles had appeared in the grain boundaries and extensive formation of terraces was observed (Fig. 2B). Fig. 3 shows SEM images of the two contact areas. Characteristic structures had developed in both contacts. The contact areas on the nickel wires show exact imprints of the structures in the YSZ contact areas (Section 5.2).

5.2. SEM of the YSZ samples after TOF-SIMS and XPS analyses

After the TOF-SIMS and XPS analyses were performed, the samples were examined with SEM. It was possible to identify the exact areas where the TOF-SIMS analyses were performed and also to correlate these with the contact areas on the nickel wires. It was also possible to correlate structures such as impurity particles on sample 231i in the SEM images with similar structures in the TOF-SIMS images.

An elliptical fracture in the YSZ was found in the centre of the contact area on sample 231i. This has also been observed on similar samples.[11,26] In the rest of the contact area on sample 231i and on the contact area on sample 232p, the Ni and the YSZ separated without deformation. Here a hill

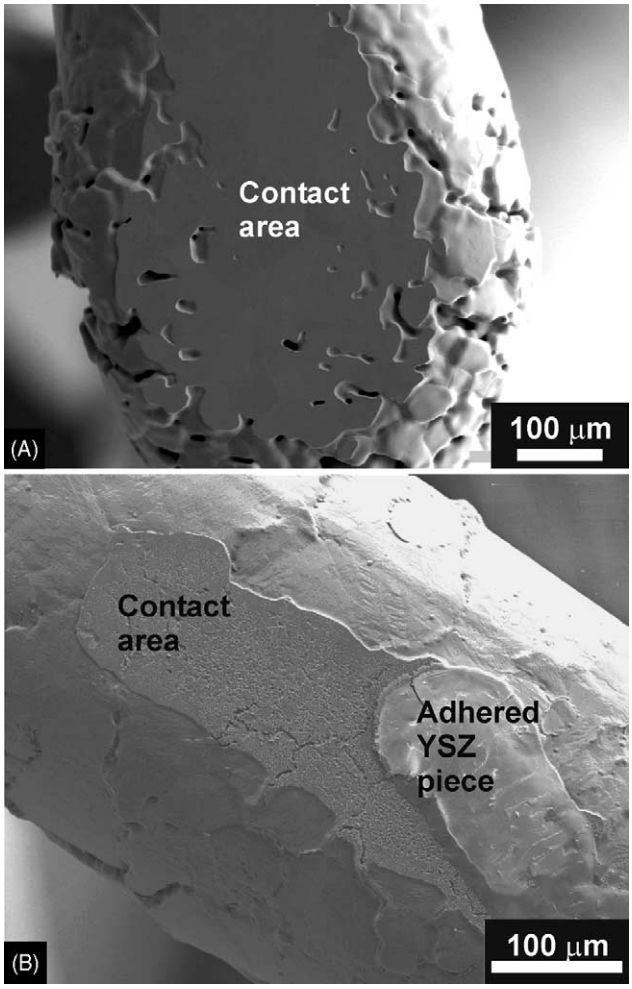

Fig. 3. Secondary electron SEM images of the two contact areas on the nickel wires after the heat treatment; (A) the pure nickel and (B) the impure nickel. The contours of the contact areas can easily be correlated with the TOF-SIMS images in Fig. 4. In (B) a part of the elliptical YSZ piece that is missing on the YSZ surface (see Fig. 4 can be seen as it is still attached to the nickel.

and valley structure had developed and an impurity ridge was found along the contact area border. The two samples did not differ from similar samples in other experiments.[11,16]

5.3. TOF-SIMS analysis

Optical images of the contact area prior to analyses showed an easily recognisable contact area on sample 231i. Visual observation of the contact area on sample 232p was not possible in the TOF-SIMS. In order to determine the exact location on the surface, a macro scan was performed with TOF-SIMS imaging covering an area of 3 mm × 3 mm. The location of the contact area was found from the contrast in the total ion signal. This analysis turned out to provide additional information, which is presented later in this section.

The number of elements that was detected with the TOF-SIMS on the YSZ and nickel reference samples exceeds by far the number of elements stated in the certificates

Table 2
TOF-SIMS (◯) and XPS (●) detected species inside and outside the contact areas the samples 232p and 231i and on the reference samples

Element	Ni wire (99.8% Ni)	Ni wire (99.995% Ni)	Sintered and polished YSZ reference sample	232p Contact area (99.995% Ni)	231i Contact area (99.8% Ni)	232p Outside the contact area (99.995% Ni)	231i Outside the contact area (99.8% Ni)
Zr			◯ ● ×	◯ ●	◯ ●	◯ ●	◯ ●
Y			◯ ● ×	◯ ●	◯ ●	◯ ●	◯ ●
Ni	◯ ● ×	◯ ● ×		◯ ●	◯	◯	◯
Si	◯ ×	◯ ×	◯ ×	◯ ●	◯ ●	◯ ●	◯ ●
O	◯ ●	◯ ●	◯ ● ×	◯ ●	◯ ●	◯ ●	◯ ●
C	◯ ● ×	◯ ●	◯ ●	◯ ●	◯ ●	◯ ●	◯ ●
Na	◯	◯	◯ ×	◯	◯ ●	◯ ●	◯ ●
N	◯ ●	◯ ●	◯	◯	◯	◯	◯
Mn	◯ ×	◯	◯	◯ ●	◯ ●	◯	◯
Ti	◯ ×	◯	◯	◯ ●	◯ ●	◯	◯
Al	◯	◯ ×	◯ ×	◯	◯	◯	◯
Fe	◯ ×	◯ ×	◯ ×	◯	◯	◯	◯
Mg	◯ ×	◯ ×	◯	◯	◯	◯	◯
Ca	◯	◯ ×	◯	◯	◯	◯	◯
Li	◯	◯	◯	◯	◯	◯	◯
B	◯	◯	◯	◯	◯	◯	◯
K	◯	◯	◯	◯	◯	◯	◯
Cr	◯	◯	◯	◯	◯	◯	◯
Pb	◯	◯ ×	◯				
F				◯	◯	◯	◯
Cu	◯ ×	◯ ×	◯				
S	◯ ×	◯					
Ag		◯ ×					
Mo		◯ ×					
Co	×						

The contents stated by the vendors are shown for the reference samples (×).

of analysis from Tosoh (YSZ) and Johnson Matthey (Ni) (compare Tables 1 and 2). The same large number of elements was also detected on the samples 231i and 232p.

The heat-treated samples show that certain elements accumulate at the surface and in the contact area. Some of the detected elements are only present in trace amounts and other elements are abundant enough to give a detailed image of the distribution. The most abundant elements are (in random order) Si, Na, Al, K, Ti, Mn, Ni, Ca, Mg and Li. Table 2 summarises the elements observed in various samples and locations. The list of TOF-SIMS detected species shown in Table 2 is the result of analysing only positive ions.

5.3.1. Large area scans

Total ion images (500 μm × 500 μm) of the contact areas on the two samples are shown in Fig. 4. The images were normalised in such that the lowest intensity measured corresponds to black and the highest intensity measured corresponds to white. Fig. 4 shows that a variation in total ion intensity was observed over the area, which is indicative of variation in surface chemistry (or physical surface properties). Furthermore, most of the individual grains can be distinguished from each other due to the intensity contrast. This suggests that the impurity layer covering the surface is extremely thin. The only exception is the contact area of

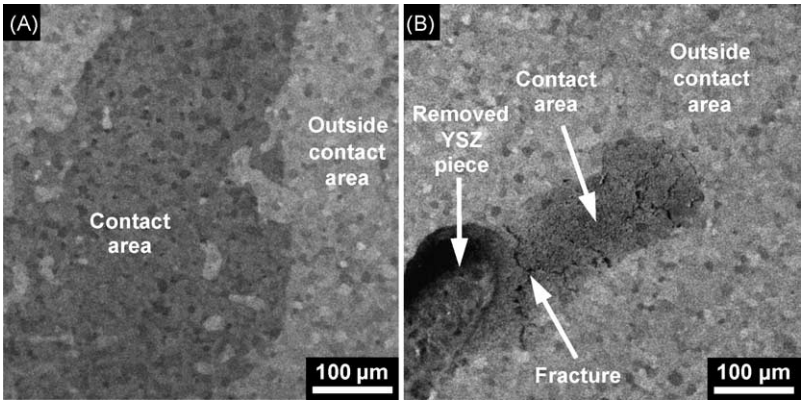

Fig. 4. TOF-SIMS total ion images (500 μm × 500 μm). High lateral resolution (~200 nm) and low mass resolution was used. Black is the lowest and white the highest total ion intensity measured. (A) The surface of sample 232p with a pure nickel wire. (B) The surface of sample 231i with an impure nickel wire.

sample 231i where a thicker layer of impurities is covering the contact area and hiding the grain structure.

In the contact area on sample 231i (Fig. 4B) a piece of the YSZ was removed when the nickel wire was removed. In spite of this hole being ∼20 μm deep (estimated by light microscopy, by focussing on top and bottom), ions are still detected from the bottom. A shadow effect caused by the fact that the primary ion beam is hitting the surface at a 45° angle is evident. This illustrates that topography affects TOF-SIMS images.

The individual ion images (500 μm × 500 μm) corresponding to the areas in Fig. 4 are presented in Figs. 5 and 6. Only components with sufficient signal intensity are displayed. The fracture after the missing YSZ piece on sample 231i is easily recognised as a black elliptical area in e.g. the Si image in Fig. 6.

The observed qualitative trend is that Li, Na, Mg, Al, Si, K, and Ca have a higher intensity outside the contact areas but for many of them some signal from the contact area is also observed. The intensity of Ti, Mn and Ni is higher in the contact area than outside the contact area. These observations are valid for both sample 231i and 232p.

The before mentioned species appear to be homogeneously distributed on the surfaces outside the contact areas, which suggests that these components are not present as a result of contamination due to handling after heating and prior to analysis.

Comparing the contact areas with the surrounding surfaces on the two samples shows that, whereas the contact area of 232p displays a high intensity from the YSZ compared to the area outside, the corresponding YSZ intensity on sample 231i is either lower or comparable with the YSZ intensity outside the contact area. These observations imply that the contact area on sample 231i and the areas outside the contact areas (on both samples) are covered with foreign elements.

The 3 mm × 3 mm scan on sample 232p revealed a few interesting new phenomena except for the location of the contact area (Fig. 7). The top right corner of each image almost corresponds to the edge of the YSZ pellet. It is normal to observe a loss of signal intensity near an edge. As is evident from Fig. 7A a gradient of silicone intensity is observed from the edge of the YSZ pellet towards the centre of the pellet. This is a well-known phenomenon. Silicone is the most commonly observed surface contaminant especially when TOF-SIMS is employed. Silicone is known to migrate effectively across surfaces. This explains the observation, since the YSZ pellet was probably handled with tweezers on the sides. The silicone image also confirms that the silicone did not reach

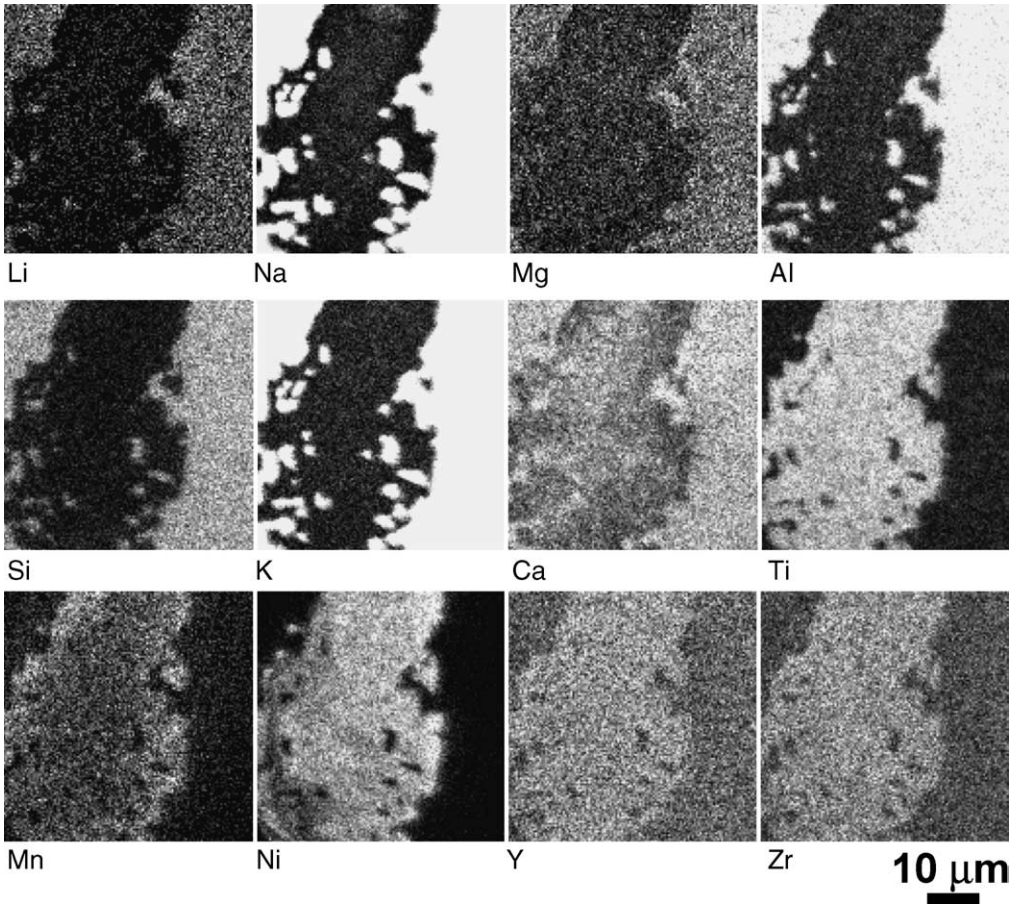

Fig. 5. TOF-SIMS ion images (500 μm × 500 μm) of the surface of sample 232p corresponding to Figs. 3A and 4A. High mass resolution and low lateral resolution was used. Black is the lowest and white the highest ion intensity measured.

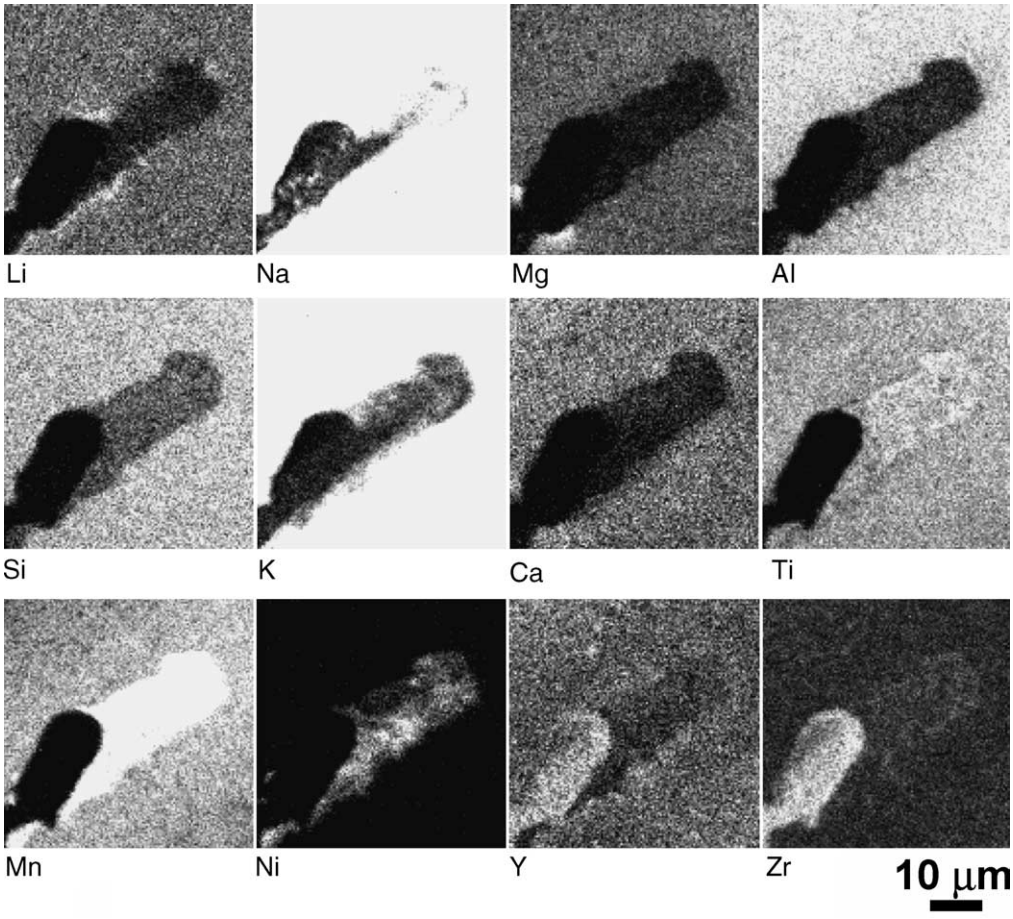

Fig. 6. TOF-SIMS ion images (500 μm × 500 μm) of the surface of sample 231i corresponding to Figs. 3B and 4B. High mass resolution and low lateral resolution was used. Black is the lowest and white the highest ion intensity measured. The dark elliptical area in e.g. the Si image is a hole created by the removal of a piece of YSZ in connection with removal of the nickel wire (see Fig. 3B).

the contact area before the analysis was performed. The most interesting observation in Fig. 7 is the Mn image (B), where the Mn signal intensity is greater in the contact area boundary region. This is supported by the intensity line profile in the Mn image, which suggests that Mn is mainly accumulated in this location. This observation is only slightly evident from Fig. 5. A subtle inhomogeneity in the distribution of Ca was observed (Fig. 7C). There is no obvious reason for this.

5.3.2. Small area scans

It is necessary to scan smaller areas in order to study the distribution of elements on a smaller scale. Fig. 8 shows 50 μm × 50 μm scans at a location near the centre of the contact area on sample 231i (A and B), at the contact area border on sample 231i (C and D), and finally, at a location near the centre of the contact area on sample 232p (E and F). The images are colour coded so that the distribution of

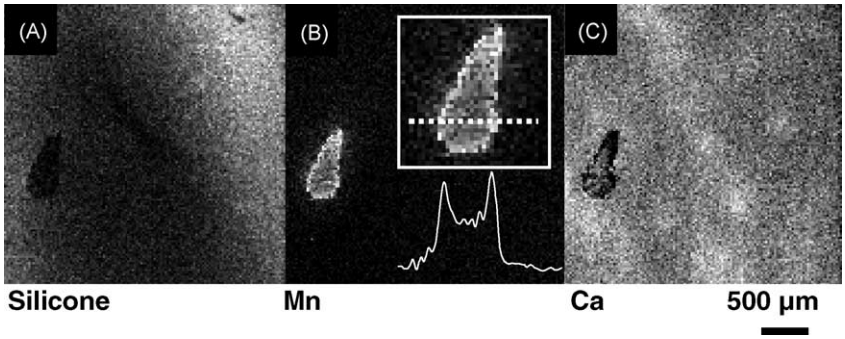

Fig. 7. TOF-SIMS ion images of (A) silicone, (B) Mn and (C) Ca from the 3 mm × 3 mm scan of sample 232p. High mass resolution and low lateral resolution was used. Black is the lowest and white the highest ion intensity measured. The insert in the Mn ion image (B) shows where the line intensity profile (below the insert) was taken. The line profile shows that the Mn is mainly accumulated at the boundary between the contact area and the outside area.

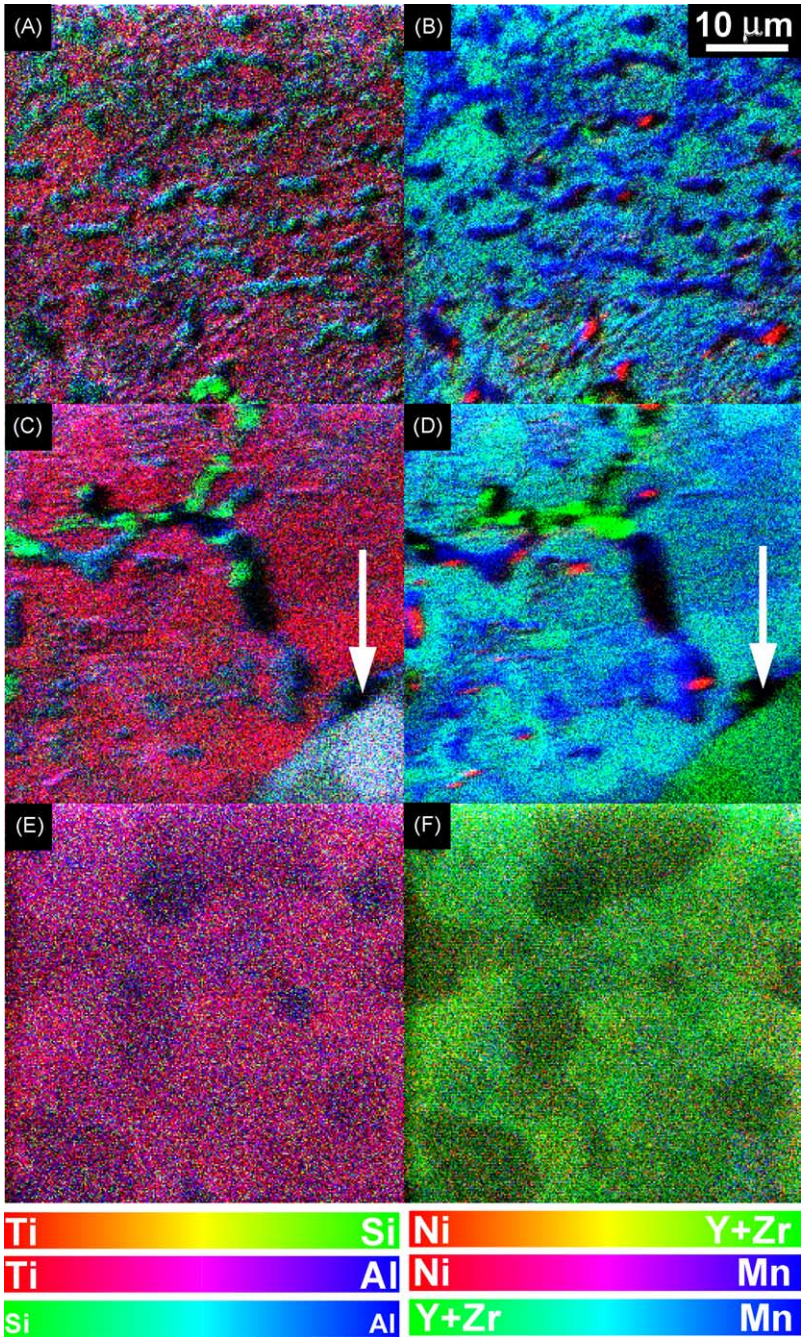

Fig. 8. TOF-SIMS combined ion images (50 μm × 50 μm). High lateral resolution (∼200 nm) and low mass resolution was used. The colours visualize the lateral distribution of the individual components; (A) and (B) are from the same area approximately in the centre of the contact area on sample 231i. Impurity particles are seen; (C) and (D) are from an area at the contact area border on sample 231i (the right lower corner is outside the contact area). The arrows show the location of the impurity ridge at the three-phase boundary; (E) and (F) show the centre of the contact area on sample 232p.

three elements can be shown simultaneously in each image. Fig. 8A, C and E display the distribution of the elements Ti, Si and Al. Fig. 8B, D and F display the elements Ni, Mn and Y + Zr.

Fig. 8A and B reveal the presence of impurity particles in the contact area of sample 231i. At the lateral resolution used (∼200 nm) for these measurements, the signal intensities are very weak, resulting in a difficulty in observing an adequate chemical contrast between the impurity particles and the substrate. It is therefore difficult, for some species, to determine whether or not these are a part of the impurity particles. A few conclusions regarding this can nevertheless be made. The impurity particles shown in Fig. 8A and B contain for certain Al and Mn, and probably also Na and K. The impurity particles contain, according to the TOF-SIMS analysis, no Ti, Ni, Y and Zr.

The contact area border is very well defined as is seen in Fig. 8C and D (arrows). Both images, even though they display only a few of the present elements, show that the surface beneath the impurity particles is covered more or less with impurities. The area outside the contact area is clearly also covered with impurities (Fig. 8C and D).

In Fig. 8D a few areas show relatively pure YSZ (green areas). It is believed that in these areas the impurity particles adhered to the nickel wire after removal of the wire from the contact area. An SEM/EDS analysis of the nickel wire supports this hypothesis.

Fig. 8B and D show that Ni is present in localized spots as particles apparently both in the centre of the contact area (B) and at the contact area boundary (D).

Fig. 8E and F are images of an area in the approximate centre of the contact area of sample 232p. Ti is distributed homogeneously over the contact area. Ni was not observed in Fig. 8F despite the fact that the 500 μm × 500 μm scan showed the presence of Ni in the contact area.

In Fig. 8F the lateral distribution of intensities is clearly inhomogeneous. The inhomogeneity is to some extend equivalent with the total ion image (not shown) but they are not consistent with each other. To study this phenomenon further, a TOF-SIMS image analysis was performed on a 50 μm × 50 μm area outside the contact area on sample 232p (Fig. 9).

Fig. 9A is a total ion image where the individual grains can be distinguished from each other, consistent with the observation in Fig. 4.

The detected ions with sufficient signal intensity are distributed in more or less three different patterns. In order to enhance the contrast of the ion images, components that have the same distribution pattern were added together. The combined sets of summed and normalized ion images are shown in Fig. 9B.

As is evident, Fig. 9B is composed of mainly three shades; a purple shade where K, Ti, Ca, Al and Na dominate; a cyan shade where Y, Zr, Ca, Al and Na dominate; and an orange shade where K, Ti, Y and Zr dominate. A certain grain surface composition do, however, not correlate with a specific grey tone in the total ion image. The grains marked “1” and “2” have according to Fig. 9B presumably identical surface chemistry, i.e. they are both purple, but according to the total ion image (Fig. 9A) the total ion signals are significantly different.

Comparing the grains “3” and “4” in Fig. 9 illustrates that two grains with different surface chemistry can produce the same total ion signal intensity. To complicate things even more, if the grains “1” and “4” (or the grains “2” and “3”) are compared it is not possible to conclude anything since these have different surface chemistry and different total ion signal intensities.

5.4. XPS analysis

Na and Si were detected outside the contact area on both samples. They amount to 39% and 28% of the cations outside the contact areas on the samples 231i and 232p, respectively. The other cations are Y and Zr. In the contact area on sample 231i, Si, Mn, Ti and Na were detected. The impurity cations amount to 54% of the total cations in the contact area. Si, Mn and Ti were also found in the contact area on sample 232p but in lower concentrations than on sample 231i. Na was not found in the contact area, but Ni was. The impurities amount to 28% of the total cations (Ni is not included).

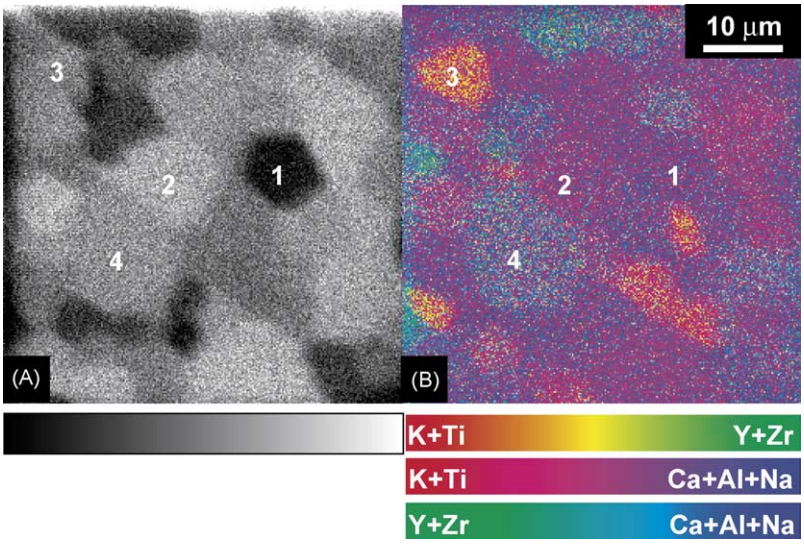

Fig. 9. TOF-SIMS ion image (50 μm × 50 μm) outside the contact area on sample 232p. High lateral resolution (∼200 nm) and low mass resolution was used. (A) Shows the total ion image. The grey-scale bar indicates the intensity, where black is the lowest and white the highest ion intensity measured. (B) Shows combined and summed ion images. Each set of images was normalized against the total ion image. The colours visualize the lateral distribution of the summed set of components.

Table 3
The element concentrations relative to Zr are shown to compare between the different samples

Element ratios	Sintered and polished YSZ pellet	232p Contact area (99.995% Ni)	231i Contact area (99.8% Ni)	232p Outside (99.995% Ni)	231i Outside (99.8% Ni)
Y/Zr	0.20 ± 0.02	0.29 ± 0.02	0.43 ± 0.05	0.37 ± 0.01	0.35 ± 0.03
Ni/Zr	0.0	0.11 ± 0.03	0.0	0.0	0.0
Si/Zr	0.0	0.22 ± 0.09	0.65 ± 0.08	0.35 ± 0.02	0.60 ± 0.03
O/Zr	2.71 ± 0.28	4.29 ± 0.23	6.78 ± 0.70	5.48 ± 0.17	6.63 ± 0.30
C/Zr	3.49 ± 0.19	2.61 ± 0.17	2.78 ± 0.31	2.24 ± 0.12	2.14 ± 0.16
Na/Zr	0.0	0.0	0.18 ± 0.07	0.19 ± 0.07	0.26 ± 0.09
Mn/Zr	0.0	0.03 ± 0.02	0.46 ± 0.08	0.0	0.0
Ti/Zr	0.0	0.07 ± 0.02	0.39 ± 0.06	0.0	0.0

The ratios are calculated from the quantitative XPS results. On the sintered and polished YSZ pellet no impurities except for carbon are found, whereas on the samples 232p and 231i a number of impurities have been detected.

To compare the concentration of elements between the samples and the different areas, element compositions relative to Zr are shown in Table 3. The Y/Zr ratio for the reference sample is 0.20, which correlates well with the ratio of 0.17 for 8 mol% YSZ. The heat-treated samples show enlarged Y/Zr ratios around 0.3–0.4 both in and outside the contact area.

Si was not detected on the reference sample. After the heat treatment the Si/Zr ratio had increased on both the samples 231i and 232p. There is no significant difference between the Si/Zr ratios when the contact areas are compared with the areas outside for the respective samples but there is a difference between the samples. The Si/Zr ratio of sample 232p is ∼0.3 and sample 231i has a Si/Zr ratio of ∼0.6.

Trace levels of sodium were found on all surfaces except in the contact area of 232p. Manganese and titanium were XPS detectable in both contact areas, but whereas the two elements were present in very small quantities on sample 232p, a significant amount was found on sample 231i, resulting in a Mn/Zr ratio of 0.46 and a Ti/Zr ratio of 0.39 (Table 3). Trace amounts of nickel were found in the contact area of sample 232p.

6. Discussion

The combined TOF-SIMS and XPS analyses have shown new results that may turn out to be very important for the interpretation of the performance of SOFC anodes. This is the first time a lateral distribution of elements near a TPB has been studied in such detail. During the TOF-SIMS measurements an enormous amount of data is accumulated and interpreting them requires very careful considerations.

Due to the significant difference in detection limits between XPS and TOF-SIMS, a large number of species detected with TOF-SIMS was not detected using XPS. Nineteen different elements are listed for the polished reference sample but only four were detected with XPS (Y, Zr, O and C). The TOF-SIMS of the nickel wires showed also the presence of many elements of which several are not indicated in the certificate of analysis from the vendor (Table 1). Since the same trace elements were detected on the reference sample most of them cannot be used to trace the origin of elements in the contact areas. Approximately the same elements are detected by the TOF-SIMS on the heat-treated samples.

The XPS measurements indicated different impurity concentrations in the two contact areas. This is plausible since the impure nickel wire contains a higher concentration of impurities (Table 1) and as a consequence will contribute more to the accumulation of impurities at the Ni–YSZ interface. It has been suggested[27] that segregation of impurities occurs due to a decrease in the free energy of the system (strain energy, electrostatic energy, surface energy) where the interface, TPB and YSZ external surface represent locations that are more energetically favourable than the bulk of the materials.

The deviation of the surface chemistry from the nominally designed composition needs to be studied in order to find methods to avoid the problems it causes. Some of the most interesting elements regarding a possible blocking layer is Si and Na since Na silicates can form glassy phases at relatively low temperatures.[28] Other elements may enter this phase and change its properties. Y^{3+} is also suggested as a constituent of the silicate phase. However, a lot of literature studies are performed with XPS, which probes such a large depth that the very surface near composition may be difficult to determine. It is argued that it is the subsurface,[29] which is enriched in Y and not the outermost layer.

Our study shows that the Y/Zr ratios for the heat-treated samples are all significantly higher than the corresponding value for the YSZ powder.

It is a reasonable assumption that matrix effects are the same for yttrium and zirconium. This makes it possible to compare the relative yttrium and zirconium intensity from the bulk via the previously mentioned hole (Fig. 4) with the corresponding intensity outside the contact area. The $^{89}Y/^{94}Zr$ intensity ratio outside the contact area is 6.6, compared to a value of 2.8 in the hole, i.e. in the bulk, indicating that yttrium has segregated to the outermost surface during the heat treatment.

The surface of sample 231i has a significantly higher content of Si than sample 232p. Since the silicon contribution from the YSZ powder was the same in the two cases, it

indicates that the impure nickel wire contributes with some silicon. In Table 1 it is found that the impure nickel wire contains a significant amount of Si. EDS analysis of the impurity particles on the impure nickel confirms that Si segregates out of the nickel during heat treatment and accumulates in particles (Fig. 2B) containing ca. 60 wt.% Si.[11,16,26] These particles also appear in the Ni–YSZ interface and so the Si is transferred from the Ni to the interface.[26] From there segregation to the YSZ surface seems to have taken place. Si segregation in YSZ has been described in many studies from the literature.[13,15,23,24,28,30–32] We have not encountered any papers describing a contribution from the nickel to the segregation process.

Sodium was, like silicon, not XPS detectable on the reference sample or in any of the nickel wires, but was detectable on the YSZ surfaces of sample 231i and 232p. This suggests that the Na impurities in the bulk must have segregated to and accumulated at the YSZ surface during heating. This phenomenon is also described in the literature[15,24,33,34] and is especially well documented with LEIS.[23] Sodium is a typical contaminant from the surroundings and a small amount of the sodium may be due to contamination during sample preparation and handling before the experiment. No possible sources of sodium contamination during and after the experiment have been identified.

From the TOF-SIMS and the XPS measurements the presence of Ti and Mn in both contact areas was established. Ti and Mn are constituents of the impure nickel and their presence in the contact area on sample 231i is thus easily explained. Ti and Mn were also detected outside the contact area with the TOF-SIMS and it is thus probable that they migrated from the interface region and to the YSZ surface.

Mn and Ti were also found on sample 232p but were not mentioned in the chemical analysis of the pure nickel from the vendor. This implies that the Ti and Mn are either present in the pure nickel in concentrations below the detection limit of the vendor's analytical method and/or that they are introduced during fabrication. Manganese and titanium were detected by TOF-SIMS on the surface of the reference sample and in the pure nickel wire, but the accumulation of Mn and Ti in the contact area suggests that the nickel is the main contributor. The Mn may migrate from the Ni surface to the TPB where a higher intensity was observed.

Ca is not stated in the chemical analysis of the YSZ from Tosoh Corporation (Table 1) but was detected on the YSZ surface. Ca has, however, been found on YSZ surfaces under such circumstances.[23,24] Due to overlap between Ca and Zr it is not possible to detect Ca on YSZ samples with the XPS. An alternative would be to use XAES or AES for the detection of Ca.

In earlier publications[11,16,26] it was shown that impurities accumulated in a ridge along the three phase boundary, both for samples with 99.8% nickel and 99.995% nickel. Different magnitudes of the ridges were found, depending on the impurity content of the nickel wire. Impurity particles were also found in the contact areas. It was then found that the impurities in the contact area consist of Na, Mg, Al, Si, K, Ti and Mn, which is in agreement with the findings in this study. Furthermore, it was possible to correlate even small structures from the SEM images with the TOF-SIMS images. The origin of the impurity particles in the contact area has been discussed elsewhere.[11,16,26]

The impurity phase on samples with 99.8% Ni was classified as an alkali silicate glassy phase possibly containing some yttrium.[11] However, the TOF-SIMS analysis did not detect any yttrium in the impurity particles.

The TOF-SIMS analysis has added the information that between or beneath the impurity particles an impurity film, more or less covering the contact area, is present. The previously used EDS technique could not establish the presence of this film or of the film on the YSZ surface outside the contact. With SEM/EDS an impurity ridge and some impurity particles were detected on sample 232p. The TOF-SIMS analysis of the contact area was performed in an area without any such particles.

The TOF-SIMS enabled us to study the distribution of elements on different scales as evidenced by the large and small area scans. From Figs. 5–8 it is evident that on a 500 μm × 500 μm scale the surface chemistry both in and outside the contact areas seems homogeneously distributed, but on a 50 μm × 50 μm scale the picture is completely different. The study (Fig. 9) on the inhomogeneous distribution of elements on different grain surfaces compared with the different signal intensities from the grains in total ion images show really the complicated nature of the chemical composition of the surfaces.

The TOF-SIMS images of the YSZ surface show the YSZ grain structure. The YSZ surface consists of many small crystals with a random distribution of crystallographic orientations. Each crystallographic orientation has its own property due to the configuration of the atoms in the facet. The secondary ion yield for the specific grains may be affected by the physical surface properties of the crystallographic orientation of the grains. This could be the reason for the different contrasts between the YSZ grains in Figs. 4 and 9A. Since the different facets have different atom configurations, different surface energies will be associated with each grain, and the grain surfaces will have different affinities for various species. Thus, different types of species may preferentially adsorb on different grains. The inhomogeneous distribution of impurities on the grains in Fig. 9B might be explained in this way. Adsorbed species on a surface may change the properties of the surface and cause adsorption of new species.

The TOF-SIMS is capable of analysing elemental distributions on a very fine scale and the analyses show that the Ni–YSZ interface is clearly a complex system that deserves further investigation. Ongoing work focuses on a dynamic TOF-SIMS study on single crystal YSZ with a better-defined Ni electrode. Dynamic TOF-SIMS provides in-depth information via depth profiling.

The TOF-SIMS technique is very suitable for imaging the distribution of elements in the Ni–YSZ interface. However, the method is not quite good enough for studying impurities in the grain boundaries and similar nano-scale structures. TEM is the method with the best resolution, but preparing a sample for this from the contact area or the very surface-near layers is very difficult.

Indeed many new details on the impurity distribution have been discovered compared to the earlier used SEM/EDS technique and direct correlation between structures was possible.

7. Conclusion

Using TOF-SIMS and XPS it has been shown that impurities accumulate at the YSZ surface and at the Ni–YSZ interface. Differences between the two samples and between contact areas and YSZ surface were found, and a contribution from impurities in the nickel was clearly observed. In an SOFC context knowing which impurities are present in the surface film and at the interface may help solve the anode performance problems. The TOF-SIMS has determined the lateral distribution of elements on different scales and showed that inhomogeneities may exist when the surface is studied on a smaller scale even though the elemental distribution seems homogeneous on a larger scale.

We have demonstrated the versatility of TOF-SIMS as an analytical tool for studying segregation phenomena at Ni–YSZ interfaces. The extremely low detection limit, the small probe depth, the image capability, and the ease of elemental identification make TOF-SIMS an obvious choice as an analytical tool for studying segregation phenomena at Ni–YSZ interfaces, and chemistry of ceramic surfaces in general. XPS has proven to be a useful complementary technique to TOF-SIMS.

Acknowledgments

K. Vels Hansen acknowledges The Nordic Energy Research Programme and M. Moggensen the Danish Energy Research Program, Project DK-SOFC b, long-term SOFC development, Project no. ENS-1713/02-0001.

References

1. Minh, N. Q. and Takahashi, T., *Science and Technology of Ceramic Fuel Cells*. Elsevier, 1995.
2. Singhal, S. C., *Solid State Ionics*, 2000, **135**, 305–313.
3. Mogensen, M. and Skaarup, S., *Solid State Ionics*, 1996, **86–88**, 1151–1160.
4. Mogensen, M., Sunde, S. and Primdahl, S., SOFC anode kinetics. In *Proceedings of the 17th Risø International Symposium on Materials Science*, ed. F. W. Poulsen, N. Bonanos, S. Linderoth, M. Mogensen and B. Zachau-Christensen, 1996, pp. 77–100.
5. Völkl, J. and Alefeld, G., Diffusion of hydrogen in metals. In *Hydrogen in Metals I*, ed. G. Alefeld and J. Völkl. Springer-Verlag, Berlin, 1978, pp. 321–348.
6. Switendick, A. C., *Berichte der Bunsen Gesellschaft*, 1972, **76**, 535–542.
7. Wagner, C., *Berichte der Bunsen Gesellschaft*, 1968, **72**, 778–781.
8. Kreuer, K. D., Proton-conducting oxides. In *Annual Reviews of Materials Research*, *Vol* 33, ed. K. D. Kreuer, D. R. Clarke, M. Rühle and J. C. Bravman. Annual Reviews, Palo Alto, CA, USA, 2003, pp. 333–359.
9. Mogensen, M., Vels Jensen, K., Jørgensen, M. J. and Primdahl, S., *Solid State Ionics*, 2002, **150**, 123–129.
10. Liu, Y.-L., Primdahl, S. and Mogensen, M., *Solid State Ionics*, 2003, **161**, 1–10.
11. Vels Jensen, K., Primdahl, S., Chorkendorff, I. and Mogensen, M., *Solid State Ionics*, 2001, **144**, 197–209.
12. Vels Hansen, K., Norrman, K. and Mogensen, M., *J. Electrochem. Soc.*, 2004, **151**, 1436–1444.
13. Hughes, A. E., Interfacial phenomena in Y_2O_3–ZrO_2-based ceramics: a surface science perspective. In *Science of Ceramic Interfaces II*, ed. J. Nowotny. Elsevier, 1994, pp. 183–238.
14. Badwal, S. P. S. and Drennan, J., Interfaces in zirconia based electrochemical systems and their influence on electrical properties. In *Science of Ceramic Interfaces II, Materials Science Monographs 81*, ed. J. Nowotny. Elsevier, 1994, pp. 71–111.
15. Badwal, S. P. S. and Hughes, A. E., Modification of cell characteristics by segregated impurities. In *Proceedings of the 2nd International Symposium on Solid Oxide Fuel Cells*, ed. P. Grosz, P. Zegers, S. C. Singhal and O. Yamamoto, 1991, pp. 445–454.
16. Vels Jensen, K., Wallenberg, R., Chorkendorff, I. and Mogensen, M., *Solid State Ionics*, 2003, **160**, 27–37.
17. Tricker, D. M. and Stobbs, W. M., Microstructural aspects of lanthanum zirconate formation. In *Proceedings of the 14th Risø International Symposium on Materials Science*, ed. F. W. Poulsen, J. J. Bentzen, T. Jacobsen, E. Skou and M. J. L. Østergård, 1993, pp. 453–460.
18. Appel, C. C., Botton, G. A., Horsewell, A. and Stobbs, W. M., *J. Am. Ceram. Soc.*, 1999, **82**, 429–435.
19. Appel, C. C. and Bonanos, N., *J. Eur. Ceram. Soc.*, 1999, **19**, 841–851.
20. Badwal, S. P. S., Drennan, J. and Hughes, A. E., Segregation in oxygen-ion conducting solid electrolytes and its influence on electrical properties. In *Science of Ceramic Interfaces, Materials Science Monographs 75*, ed. J. Nowotny. Elsevier, Amsterdam, 1991, pp. 227–279.
21. Briggs, D., *Surface Analysis of Polymers by XPS and Static SIMS*. Cambridge University Press, 1998.
22. Vickerman, J. C. and Briggs, D., *TOF-SIMS Surface Analysis by Mass Spectrometry*. IM Publications and SurfaceSpectra Limited, 2001.
23. de Ridder, M., van Welzenis, R. G., Brongersma, H. H., Wulff, S., Chu, W.-F. and Weppner, W., *Nucl. Instrum. Methods Phys. Res. B*, 2002, **190**, 732–735.
24. de Ridder, M., Vervoort, A. G. J., van Welzenis, R. G. and Brongersma, H. H., *Solid State Ionics*, 2003, **156**, 255–262.
25. Brongersma, H. H., Groenen, P. A. C. and Jacobs, J.-P., Application of low energy ion scattering to oxidic surfaces. In *Science of Ceramic Interfaces II*, ed. J. Nowotny. Elsevier, 1994, pp. 113–182.
26. Vels Jensen, K., *The Nickel–YSZ Interface—Structures, Composition and Electrochemical Properties at 1000 °C*. Thesis, Risø National Laboratory, Denmark, 2002.
27. Burggraf, A. J. and Winnubst, A. J. A., Segregation in oxide surfaces, solid electrolytes and mixed conductors. In *Surface and Near-surface Chemistry of Oxide Materials*, ed. J. Nowotny and L.-C. Dufour. Elsevier, 1988, pp. 449–477.
28. Hughes, A. E. and Badwal, S. P. S., *Solid State Ionics*, 1991, **46**, 265–274.

29. de Ridder, M., van Welzenis, R. G., Denier van der Gong, A. W., Brongersma, H. H., Wulff, S., Chu, W.-F. *et al.*, *J. Appl. Phys.*, 2002, **92**, 3056–3064.
30. Bernasik, A., Kowalski, K. and Sadowski, A., *J. Phys. Chem. Solids*, 2002, **63**, 233–239.
31. Hughes, A. E., *J. Am. Ceram. Soc.*, 1995, **78**, 369–378.
32. Theunissen, G. S. A. M., Winnubst, A. J. A., Burggraf, A. J., *Surfaces and Interfaces of Ceramic Materials, Nato ASI Series, Series E: Applied Sciences, Vol 173*, 1989.
33. Badwal, S. P. S. and Hughes, A. E., *J. Eur. Ceram. Soc.*, 1992, **10**, 115–122.
34. Hughes, A. E. and Sexton, B. A., *J. Mater. Sci.*, 1989, **24**, 1057–1061.